

Global instability by runaway collisions in nuclear stellar clusters: Numerical tests of a route for massive black hole formation.

M.C. Vergara^{1,2,*}, A. Escala³, D.R.G. Schleicher¹, B. Reinoso⁴

¹ Departamento de Astronomía, Facultad Ciencias Físicas y Matemáticas, Universidad de Concepcion, Av. Esteban Iturra s/n Barrio Universitario, Casilla 160-C, Concepcion, Chile

² Astronomisches Rechen-Institut, Zentrum für Astronomie, University of Heidelberg, Mönchhofstrasse 12-14, 69120, Heidelberg, Germany

³ Departamento de Astronomía, Universidad de Chile, Casilla 36-D, Santiago, Chile

⁴ Universität Heidelberg, Zentrum für Astronomie, Institut für Theoretische Astrophysik, Albert-Ueberle-Str. 2, 69120 Heidelberg, Germany

* marccortes@udec.cl

October 3, 2022

ABSTRACT

The centers of galaxies host nuclear stellar clusters, supermassive black holes, or both, but the origin of this dichotomy is still a mystery. Nuclear stellar clusters are the densest stellar system of the Universe, so they are ideal places for runaway collisions to occur. In these dense clusters it is possible that global instability occurs, triggered by collisions and mergers forming a massive black hole. Here we test a new mechanism to form massive black holes through runaway stellar collisions in nuclear stellar clusters, performing N-body simulations using the code `NBODY6++GPU`. Our idealized models show that there is a critical mass where collisions become very efficient making it possible to form massive black holes in nuclear stellar clusters. The most massive objects reach masses of the order of $10^4 - 10^5 M_{\odot}$. We find that our highest black hole formation efficiency is up to 50% of the stellar mass at the end of the simulation. In real astrophysical systems, the critical mass scale for this transition is expected to occur in stellar clusters of $10^7 - 10^9 M_{\odot}$, implying the formation of quite massive central objects.

Key words. cosmology: theory — early Universe – stars: kinematics and dynamics – black hole

Use \titlerunning to supply a shorter title and/or \authorrunning to supply a shorter list of authors.

1. Introduction

There is a dichotomy at the center of most galaxies, with some galaxies hosting supermassive black holes (SMBHs) at the center (Volonteri et al. 2010; Kormendy & Ho 2013), and other galaxies harboring a Nuclear Star Cluster (NSC) (Böker et al. 2002; Côté et al. 2006). In addition the presence of NSCs surrounding SMBHs is also observed. Any SMBH or/and NSC in the galaxy center is usually called a Central Massive Object (CMO) (Ferrarese et al. 2006; Georgiev et al. 2016; Neumayer et al. 2020). Nuclear star clusters are the densest stellar configurations in the Universe with masses of $\sim 10^6 - 10^7 M_{\odot}$ (Walcher et al. 2005), while supermassive black holes are the densest objects in the Universe with masses of $\sim 10^6 - 10^{10} M_{\odot}$ (Volonteri et al. 2010; Natarajan & Treister 2009; King 2016; Pacucci et al. 2017). Additionally, there is evidence of a correlation between the mass of the SMBH and/or NSC with the properties in the host galaxy (Ferrarese et al. 2006; Wehner & Harris 2006; Li et al. 2007; Graham & Spitler 2009; Genzel et al. 2010; Leigh et al. 2012; Antonini et al. 2015). A correlation between the mass of a SMBH and the velocity dispersion of the stars around it has been observed (Ferrarese & Merritt 2000; Tremaine et al. 2002; Gültekin et al. 2009), as well as a correlation between the mass of the SMBH and the mass of the bulge of its host galaxy (Magorrian et al. 1998; Marconi & Hunt 2003; Häring & Rix 2004). On the other hand, there are also measures of a correlation between the mass of the NSC and the bulge luminosity of their host

galaxies (Wehner & Harris 2006; Côté et al. 2006; Rossa et al. 2006; Böker 2008), suggesting a possible co-evolution between the SMBH and the NSC with the host galaxy.

Recently the first image confirming the presence of the SMBH called Sagittarius A* in our Galaxy, the Milky Way (Akiyama et al. 2022) as well as studies of stellar orbits around this object (Ghez et al. 2008; Genzel et al. 2010; Gillessen et al. 2017) confirm that our galaxy has a NSC and a SMBH at its center (Genzel et al. 2010; Schödel et al. 2014). Other galaxies with NSC and SMBH are e.g. NGC 4395 (Filippenko & Ho 2003), M 31 (Bender et al. 2005), NGC 1042 (Shields et al. 2008), NGC 3621 (Barth et al. 2009), NGC 6388 (Lützgendorf et al. 2011), NGC 404 (Seth et al. 2010; Nguyen et al. 2017), NGC 3319 (Jiang et al. 2018) and NGC 3593 (Nguyen et al. 2022). Moreover, there are SMBH detections at high redshift, though it is not yet clear how they could reach large masses of $\sim 10^9 - 10^{10} M_{\odot}$ (Volonteri et al. 2010; Natarajan & Treister 2009; King 2016; Pacucci et al. 2017) within such a short time, when the Universe was just a few hundred million years old. The high-redshift SMBH observations include e.g. the detection of the first 3 quasars at $z > 6$ by Fan et al. (2003), the most massive SMBH discovered by Wu et al. (2015) with a mass of $1.2 \times 10^{10} M_{\odot}$ at $z = 6.3$, and the most distant AGN at $z = 7.5$ with a mass of $8 \times 10^8 M_{\odot}$ observed by Bañados et al. (2018). In total more than 100 quasars have been observed at $5.6 \lesssim z \lesssim 6.7$ as summarized by Bañados et al. (2016). Mortlock et al. (2011) observed a quasar at $z = 7.085$ with a mass of $2 \times 10^9 M_{\odot}$.

Although the exact process of SMBH formation is still unknown, there are several scenarios that try to explain their formation (Woods et al. 2019), such as Direct Collapse (DC) based on the presence of massive gas clouds at high redshift, which collapse in an atomic cooling halo (Bromm & Loeb 2003; Volonteri et al. 2008; Latif et al. 2013; Latif & Schleicher 2015). However, the presence of molecular hydrogen produces fragmentation in the cloud (Omukai et al. 2008; Latif et al. 2016; Bovino et al. 2016; Suazo et al. 2019). Forming a supermassive star requires input rates of $0.1 M_{\odot}/\text{yr}$ (Begelman 2010; Schleicher et al. 2013; Sakurai et al. 2015). Another scenario is based on the remnants of population III (Pop. III) stars; these stars are born in clouds with zero metallicity when the cloud collapses. The protostars accumulate material on the hydrostatic core, forming a very massive star (VMS) (Omukai & Nishi 1998; Volonteri et al. 2003; Tan & McKee 2004; Ricarte & Natarajan 2018). Another proposed scenario related to the stellar dynamics in a star cluster is runaway collisions and mergers. In this scenario, several collisions occur with a single star that eventually becomes a more massive object (Rees 1984; Devecchi & Volonteri 2009; Katz et al. 2015; Sakurai et al. 2017, 2019; Boekholt et al. 2018; Reinoso et al. 2018, 2020; Alister Seguel et al. 2020; Vergara et al. 2021; Schleicher et al. 2022).

MBHs are located in the galactic center. All surrounding gaseous material and stars will eventually lose their angular momentum as they fall into the center of the galaxy because it is the deepest gravitational zone of the stellar configuration (Shlosman et al. 1990; Escala 2006). There are multiple processes that could lead to a strong inflow, e.g. gravitational torques in the merger of galaxies (Barnes 2002; Mayer et al. 2010; Prieto et al. 2021) or migration of groups by dynamic friction (Escala 2007; Elmegreen et al. 2008) among others. At high redshift, there is a high fraction of systems with gas and no MBH (which could provide AGN feedback), suggesting that the strong inflow should be more extreme (Prieto & Escala 2016). Therefore, the densest stellar/gas configuration should be found at these locations. If these materials (gas and stars) do not form an MBH, they will probably form NSCs, which is the other stable physical configuration that can remain in the center of the galaxy (Escala 2021). NSCs are ideal places for stellar collisions to occur. Numerical simulations of clusters with masses less than $10^6 M_{\odot}$ show a low BH formation efficiency (ϵ_{BH}) of up to a few percent of the initial mass (Portegies Zwart & McMillan 2002; Devecchi & Volonteri 2009; Sakurai et al. 2017; Reinoso et al. 2018), while ϵ_{BH} grows dramatically for the most massive clusters ($10^7 M_{\odot}$). This growth is triggered by runaways stellar collisions (Lee 1987; Quinlan & Shapiro 1990; Davies et al. 2011; Stone et al. 2017).

In this paper, we explore a new scenario proposed by Escala (2021) where stellar collisions in NSCs provided a mechanism to form MBHs. We tested the scenario using N-body simulations that explore different cluster initial conditions, looking for collisionally unstable configurations that lead to a large amount of the initial mass collapsing into a MBH as predicted by Escala (2021).

The outline of the paper is the following: in section 2 we describe the proposed scenario for MBH formation. Then in section 3, we describe our models and N-body simulations. In section 4 we present our results and finally, we discuss them and our conclusions in section 5.

2. Proposed scenario for MBH formation

Escala (2021) proposed a new MBH formation scenario, motivated by showing that the observed nuclear stellar clusters are

in a regime where collisions are not relevant throughout the system; on the other hand, well-resolved observed MBHs are found in regimes where collisions are expected to be dynamically irrelevant. In this context it was shown that NSCs in virial equilibrium with masses higher than $10^8 M_{\odot}$ have short collision times, so these stellar configurations are too dense to be globally stable against collisions. This leads to a destabilization of the cluster and allows most of the mass to collapse into a central massive object.

NSCs are the densest stellar systems in nature, thus they represent one of the most favorable places for runaways collision to occur. The close encounters of the stars within the cluster generally occur at high speed in the center due to the deep gravitational potential. The gravitational interactions can lead to the ejection of stars that leave the system with some kinetic energy producing a redistribution of the energy and allowing the cluster to undergo a core collapse (Lynden-Bell & Wood 1968; Cohn 1979; Spitzer 1987). Stellar collisions are expected to occur when the cluster core collapses, causing a single object to experience almost all of the collisions, increasing exponentially in mass during the core collapse (Portegies Zwart et al. 1999; Portegies Zwart & McMillan 2002). Core collapse has an associated time known as the relaxation timescale. If the system is virialized, the crossing time is $t_{cross} = \sqrt{R^3/GM}$, where G is the gravitational constant, R and M are the radius and mass of the cluster, respectively. The crossing time quantifies the time that a star with a typical velocity needs to cross the cluster. The typical velocity is defined as the root mean square of the stellar velocities. The relaxation timescale is related to the perturbation of the global properties of the cluster such as stellar orbits, and quantifies the energy exchange between two bodies. Binney & Tremaine (2008) defined the relaxation timescale as $t_{relax} = 0.1N * t_{cross} / \ln(N)$, where N is the total number of particles.

In a cluster that has equal mass stars, the total number of stars is $N = M/M_*$, where M_* represents the mass of a single star, while the stellar radius is denoted as R_* . The occurrence of runaway collisions can be quantified through the collision timescale defined as $t_{coll} = \lambda/\sigma$, where σ is the velocity dispersion and λ is the stellar mean free path (Binney & Tremaine 2008). In a virialized system the velocity dispersion is defined as $\sigma = \sqrt{GM/R}$. Landau & Lifshitz (1980) and Shu (1991) define a probabilistic mean free path as $\lambda = 1/n\Sigma_0$, where Σ_0 is the effective cross section and n the number density of stars. Therefore the collision rate is defined as $t_{coll} = \sqrt{R/GM(n\Sigma_0)^2}$, the number density is $n = 3M/4\pi R^3 M_*$ and the effective cross section is $\Sigma_0 = 16\sqrt{\pi}R_*^2(1 + \Theta)$, where $\Theta = 9.54((M_*R_{\odot})/(M_{\odot}R_*))((100 \text{ kms}^{-1})/(\sigma))^2$ is the Safronov number (Binney & Tremaine 2008). Under the condition that the collision time is equal to or shorter than the age of the system (t_H), we can derive the following equation,

$$M \geq \left(\frac{4\pi M_*}{3\Sigma_0 t_H G^{1/2}} \right)^{2/3} R^{7/3}, \quad (1)$$

and under the condition that the relaxation time is equal to or shorter than the time t_H , we have

$$R \leq \left(\frac{t_H M_*}{0.1} \ln \left(\frac{M}{M_*} \right) \right)^{2/3} \left(\frac{G}{M} \right)^{1/3}. \quad (2)$$

Note that for $M_* = 1 M_{\odot}$, $R_* = 1 R_{\odot}$ and $\sigma = 100 \text{ km/s}$, the Safronov number is $\Theta = 9.54$, leaving a value for the effective

cross section of $\Sigma_0 \approx 100\pi R_\odot^2$. Equations 1 & 2 lead to the conditions discussed in Escala (2021)¹ in their equations 2 & 4.

The dichotomy in the centers of galaxies shows CMO, which can be MBHs and/or NSCs. The presence of NSCs is generally found in galaxies with masses less than $10^{10} M_\odot$, while MBHs are generally found in more massive galaxies with masses larger than $10^{12} M_\odot$. There is also evidence of the coexistence of both objects in galaxies with intermediate masses (Georgiev et al. 2016). It is possible that both objects are in a different phase of evolution from a common formation mechanism. If the CMO is too dense and meets the condition of having a collision time shorter than the time t_H , then the system cannot expand and becomes globally unstable against collisions, and probably collapse into a MBH. On the other hand, for less dense CMOs, the system is globally stable, allowing the presence of an NSC that probably coexists with a low-mass BH in the center (Escala 2021).

Simulations of stellar dynamics have been investigated using N-body codes for cluster masses typically smaller than $10^6 M_\odot$ (Portegies Zwart & McMillan 2002; Devecchi & Volonteri 2009; Sakurai et al. 2017; Reinoso et al. 2018). Since more massive systems are numerically expensive, these configurations have been investigated with Fokker-Planck models of galactic nuclei developed by Lee (1987); Quinlan & Shapiro (1990), which show a transition called ‘merger instability’ in the formation of the CMO at masses over or similar to $10^7 M_\odot$. However, in order to test the global instability proposed by Escala (2021), it is useful to define a critical mass (M_{crit}) as the mass at which the virial radius of our clusters crosses the collision line. This can be computed from the marginal condition in equation 1:

$$M_{crit} = R^{7/3} \left(\frac{4\pi M_*}{3\Sigma_0 t_H G^{1/2}} \right)^{2/3}, \quad (3)$$

In the next section, we will describe the initial conditions of our simulations. These are meant to provide a proof of concept for the new scenario, showing that a transition exists at the critical mass derived by Escala (2021). We note here in advance that for computational reasons, these simulations are pursued for less massive but more compact clusters considering also a shorter evolution time, as in that case, the critical mass scale is lowered and it becomes feasible to explore the transition via N-body simulations. In the real Universe, clusters are less compact but have much more time to evolve, leading to critical masses of the order $10^7 M_\odot$.

3. Model setup and simulations

Our simulations were run with `NBODY6++GPU` (Wang et al. 2015), a direct N-body code with high precision based on the codes `NBODY6++` (Spurzem 1999) and `NBODY6` (Aarseth 2000). This code includes an algorithm to solve N-body interactions as close encounters, binaries (Kustaanheimo & Stiefel 1965) or multiple systems (Mikkola & Aarseth 1990, 1993). Besides, it includes a spatial hierarchy to speed up computational calculations (Ahmad & Cohen 1973). This code works with the 4th order Hermite integrator scheme of Makino (1991) and also includes an optimization for the calculations of gravitational forces between particles using Graphics Processing Units (GPUs) (Nitadori & Aarseth 2012; Wang et al. 2015).

¹ We note a typo in eq. 2 of Escala (2021) introduced by the journal during the proofreading process: $t_{HG}^{1/2}$ in Escala (2021) should be $t_H G^{1/2}$

We consider that collisions occur when the radii of two stars overlap (i.e $D \leq R_{*1} + R_{*2}$); if the stars fulfill this condition, we replace them with a new single star (Davies et al. 1993; Freitag & Benz 2005; Alister Seguel et al. 2020) but we neglect it here as usually, the mass loss is on the percent level. The treatment adopted here in principle provides a lower limit regarding the number of collisions. The parameters of the new star after the merger are as follows:

$$M_*^{new} = M_{*1} + M_{*2}, \quad (4)$$

$$R_*^{new} = R_{*1} (1 + M_{*2}/M_{*1})^{1/3}, \quad (5)$$

which assumes that the stellar mass density remains constant. We consider that the new star reaches hydrostatic and thermal equilibrium quickly after the collision.

3.1. Initial Conditions

We are testing the new scenario of NSC instability under collisions as a mechanism to form MBHs (Escala 2021), using a Plummer (1911) distribution of equal-mass stars and evolving the clusters for a time $t_H = 10$ Myr. We also vary the initial number of stars as $N = 5 \times 10^2, 10^3, 5 \times 10^3, 10^4$ and the initial cluster virial radii as $R_v = 0.005, 0.01, 0.1, 1$ pc. The stars have an initial mass of $M_* = 1, 10, 50 M_\odot$ with a radius $R_* = 1, 4.7, 11.7 R_\odot$, respectively, computed from the mass-radius equations

$$R_* = 1.6 \times (M_*/M_\odot)^{0.47} R_\odot, \quad 10 \leq M_* < 50 M_\odot, \quad (6)$$

$$R_* = 0.85 \times (M_*/M_\odot)^{0.67} R_\odot, \quad M_* \geq 50 M_\odot, \quad (7)$$

from the relations described by Bond et al. (1984) and Demircan & Kahraman (1991), respectively.

In figure 1 we show the distribution of our models in the mass-radius parameter space. The equations 1 and 2, for $t_H = 10$ Myr are described by the orange lines for $M_* = 1 M_\odot$, magenta lines for $M_* = 10 M_\odot$ and blue lines for $M_* = 50 M_\odot$. The left side of the hatched area ($t_{coll} < t_H$) is the parameter space where collisions dominate the cluster dynamics over the whole system, while the right side ($t_{coll} > t_H$) represents the parameter space where collisions are not globally relevant. Nevertheless, in the core of the cluster the collisions occur more frequently; then the NSCs can coexist with an unstable core triggered by the Spitzer instability (Spitzer 1969; Portegies Zwart & McMillan 2002). Therefore, the collision timescales are important to determine the global instability in NSCs against runaway collisions.

Observed NSCs typically have radii of 1 – 10 pc and masses around $10^6 - 10^8 M_\odot$ (Georgiev et al. 2016), still being globally stable, since they have a collision time larger than the age of the Universe (Escala 2021) (i.e. they are one order of magnitude in mass below the line given by equation 1), so the critical mass is typically in the range $10^7 - 10^9 M_\odot$. Doing simulations in this range of NSC masses is still numerically prohibitive (for 1 – $10 M_\odot$ stars), however, we can do simulations of less massive NSCs, which are numerically less expensive when run over a shorter evolutionary period. In particular, we present here a set of simulations that crosses the collision threshold given by equation 1 to test the catastrophic dynamics of the proposed scenario. We can simulate NSCs above the line described by eq. 1

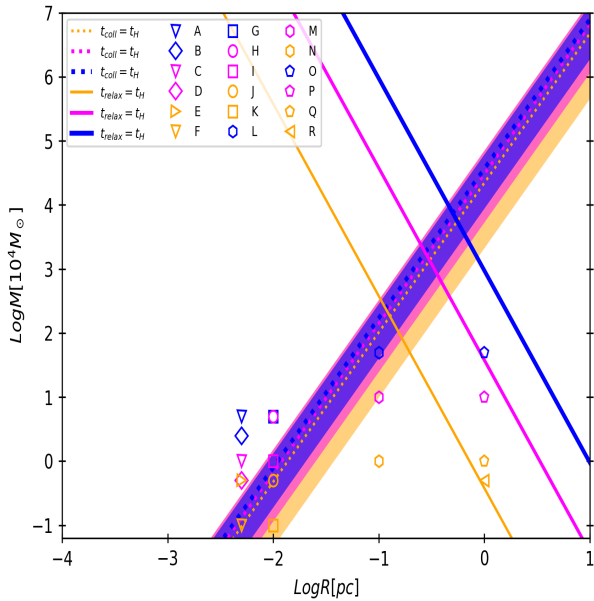


Fig. 1. The blue, magenta and orange symbols, lines and colored areas are for $M_* = 50, 10, 1 M_\odot$, respectively. Equal symbols represent the same number of stars N . Solid lines are from the condition of equation 2, dotted lines are the mean of equation 1 for the different models, and all lines for the time evolution of $t_H = 10$ Myr. The colored areas represent the range of the condition given by equation 1, for the models with different initial σ (Table 1).

(i.e. lower critical masses ($10^3 - 10^5 M_\odot$)), using a radius range of $0.005 - 0.01$ pc for a mass range of $10^3 - 10^4 M_\odot$. In addition, some of our models with a radius of $0.1 - 1$ pc have a mass from around $10^3 - 10^5 M_\odot$; this means that they are also below the line described by eq. 1, having larger critical than cluster masses, in order to check how the efficiency of forming a MBH grows as we cross the line that defines the marginal condition in equation 1).

The idealized models presented here are useful for testing the concept described by Escala (2021) and this is the first step in testing this new proposed scenario considering global instabilities in NSCs as a mechanism to form MBHs. Our models are more representative of when the NSCs are born, as the NSCs can have a radius approximately ten times smaller at the moment of formation (Banerjee & Kroupa 2017). Due to the evolution process it must be considered that the radius of the cluster expands (Baumgardt et al. 2018; Panamarev et al. 2019), moving the models from left to right.

We simulated 18 nuclear star clusters, covering different regions of the mass-radius parameters space. The empty blue symbols are for $M_* = 50 M_\odot$, empty magenta symbols for $M_* = 10 M_\odot$, and empty orange symbols for $M_* = 1 M_\odot$. It is important to note that our NSC models do not reach masses greater than 10^7 (much less with 10^7 particles). However, we can still explore this new scenario proposed by Escala (2021) via the modeling of more compact clusters for shorter time intervals. For such clusters the critical mass scale from equation 3 will be reduced, so that the computational modeling becomes feasible due to the smaller number of stars in the simulation. We summarize our initial conditions in table 1

4. Results

The initial mass of the clusters in our models is $M = N \times M_*$. The mass of the CMO can be computed as the sum of the masses of the NSC and BH ($M_{CMO} = M_{NSC} + M_{BH}$), the mass of the BH can be denoted by $M_{BH} = \epsilon_{BH} M_{CMO}$, and the mass of the surrounding stars of the NSC can be denoted as $M_{NSC} = (1 - \epsilon_{BH}) M_{CMO}$. Then the black hole formation efficiency (ϵ_{BH}) is defined as

$$\epsilon_{BH} = (1 + M_{NSC}/M_{BH})^{-1}. \quad (8)$$

From the simulation data the mass of the CMO can be calculated as $M_{CMO} = M - M_{esc}$, where M_{esc} is the cumulative mass of the ejected stars, thus

$$M = M_{CMO} + M_{esc} = M_{NSC} + M_{BH} + M_{esc}. \quad (9)$$

4.1. Simulated star cluster evolution

In this subsection, we analyze the time evolution of the cumulative mass of stars that escape from the system, the growth of mass of the most massive object, the black hole formation efficiency, and the Lagrangian radii at 90%, 50%, and 10%.

We analyze the evolution of two models B and M. Model B has $M = 2.5 \times 10^4 M_\odot$, with a virial radius of 0.005 pc. Model M has an initial mass of $10^5 M_\odot$, with $R_v = 1$ pc. Model B is in the region where collisions dominate the stellar dynamics (i.e. $t_{coll} < t_H$). Model M is in the region where collisions are not relevant over the whole system (i.e. $t_{coll} > t_H$). We present the cumulative mass of escapers normalized by the initial mass M , the number of collisions normalized by the initial number of stars N , the black hole formation efficiency ϵ_{BH} described by equation 8 and the Lagrangian radii corresponding to 90%, 50%, and 10% of the enclosed mass.

In Fig. 2 we show the evolution of model B over 1 Myr. The top panel shows the cumulative mass of stars escaping from the

Table 1. The virial radius is R_v , M is the initial mass of the cluster, N is the initial number of stars, the stellar mass and radius is M_* and R_* , respectively, and σ is the velocity dispersion.

Models	R_v	M	N	M_*	R_*	σ
ID	[pc]	[M_\odot]		[M_\odot]	[R_\odot]	[km/s]
A	0.005	5×10^4	10^3	50	11.7	207.38
B	0.005	2.5×10^4	5×10^2	50	11.7	146.64
C	0.005	10^4	10^3	10	4.7	92.74
D	0.005	5×10^3	5×10^2	10	4.7	65.58
E	0.005	5×10^3	5×10^3	1	1	65.58
F	0.005	10^3	10^3	1	1	29.32
G	0.01	5×10^4	10^3	50	11.7	146.64
H	0.01	5×10^4	5×10^3	10	4.7	146.64
I	0.01	10^4	10^3	10	4.7	65.58
J	0.01	5×10^3	5×10^3	1	1	46.37
K	0.01	10^3	10^3	1	1	20.73
L	0.1	5×10^5	10^4	50	11.7	146.64
M	0.1	10^5	10^4	10	4.7	65.58
N	0.1	10^4	10^4	1	1	20.73
O	1	5×10^5	10^4	50	11.7	46.37
P	1	10^5	10^4	10	4.7	20.73
Q	1	10^4	10^4	1	1	6.55
R	1	5×10^3	5×10^3	1	1	4.63

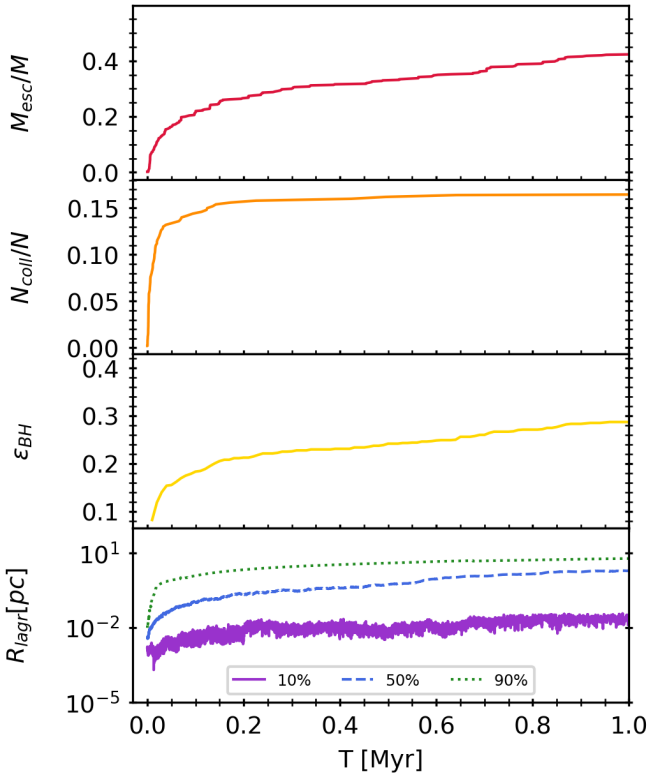


Fig. 2. Evolution of model B for 1 Myr. Top panel: The cumulative mass of escapers normalized by the initial mass M . First middle panel: The number of collisions normalized by the initial number of stars N . Second middle panel: The black hole formation efficiency ϵ_{BH} described by equation 8. Bottom panel: Lagrangian radii for the 10%, 50%, and 90% of the enclosed mass.

cluster normalized by the initial mass M ; the stellar cluster has lost around 42% of the initial mass after 1 Myr. The first middle panel shows the total number of collisions N_{coll} normalized by the initial number of stars $N = 500$; until 1 Myr 82 collisions have occurred. The second middle panel shows the black hole formation efficiency ϵ_{BH} reaching a value of around 28%. The stellar system forms a single massive object of $4150 M_{\odot}$. The bottom panel shows the Lagrangian radii at 90%, 50%, and 10% of the enclosed mass. The outer zone of the stellar system corresponding to 90% of the mass shows an expansion until around 0.1 Myr, then remains almost constant. The middle zone corresponding to 50% of the mass shows a smooth expansion all the time while the inner zone at 10% of the enclosed mass shows a decrease at the beginning of the simulation.

In Fig. 4.1 we display the evolution of the same model B over 10 Myr. The panels are the same as in Fig. 2. The top panel shows that around 58% of the initial mass is lost. The first middle panel shows that 85 collisions in total occurred, most collisions happened in the first Myr. The most massive object reaches a mass of $4300 M_{\odot}$. The second middle panel shows that the black hole formation efficiency increases until a value of 41%. After 2 Myr, the 90% and 50% Lagrangian radii curves start to overlap because there is so much mass loss. The 10% Lagrangian radius shows a rapid decrease at first followed by an expansion and then remains almost constant.

Comparing Fig. 2 and Fig. 4.1, after 9 Myr, the cumulative mass of stars escaping from the star system increases by 16%. The number of collisions increases only a bit meaning that the most massive object reaches a mass of $4300 M_{\odot}$. The black hole

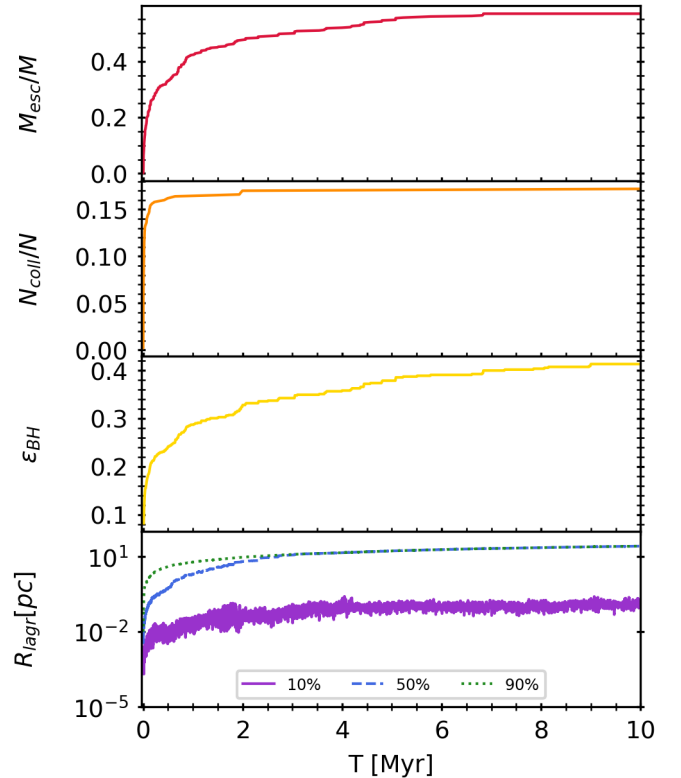


Fig. 3. Evolution of model B for a time period of 10 Myr. Panels are the same as in Fig. 2.

formation efficiency ϵ_{BH} increases by 13%; this increase is more due to the escapers than the collisions since the mass of the most massive object increases only by $150 M_{\odot}$ while there are several stars that escape from the stellar system.

Model B is one of the densest models. This model is very chaotic, showing a contraction at the beginning. Almost all collisions occur within 1 Myr; there are also several escapers during this time, therefore the black hole formation efficiency increases due to both processes. After 1 Myr only a few collisions occur, while the number of escapers continues to increase. This means that during the late times the increase of ϵ_{BH} is dominated more by the number of escapers than by stellar collisions. This may explain that in some of the observed systems a star cluster is no longer visible.

Fig. 4 shows the evolution of model M over 3 Myr. The panels are the same as in Fig. 2. The top panel shows that after 3 Myr 220 stars of $10 M_{\odot}$ have escaped from the cluster. The first middle panel shows that around 140 collisions occurred during this time. The second middle panel shows that the black hole formation efficiency is very low; after 3 Myr it reaches a value of less than 2%. The most massive object reaches a mass of $1670 M_{\odot}$. The Lagrangian radii at 90% and 50% remain almost constant, while the Lagrangian radius at 10% shows a smooth decrease until 2.5 Myr when a contraction occurs, followed by an expansion. After 2.5 Myr there is an increase in the number of escapers from the system. An increase in the number of collisions also occurs, several of them with the most massive object, and the black hole formation efficiency also increases after 2.5 Myr.

We show the evolution of this model until 3 Myr. Until the time of 1 Myr, the number of collisions and escapers is very low, so it is not quite interesting. Model M has a long relaxation time ($t_{relax} \approx 0.16$ Myr), so it takes longer for the collapse to occur,

the time of core collapse is $t_{cc} \propto 20t_{relax}$, around this time the collisions are triggered and therefore the mass growth of the BH begins.

Fig. 5 shows the evolution of model M for a time period of 10 Myr. The panels are the same as in Fig. 2. The top panel shows that around 8% of the stellar mass is lost due to the escapers. The first middle panel shows around 700 stellar collisions. The most massive object reaches a mass of $6700 M_{\odot}$. The second middle panel shows that the black hole formation efficiency reaches a value of 7%. The Lagrangian radius at 90% shows an expansion over time, the Lagrangian radius at 50% remains almost constant while the Lagrangian radius at 10% shows a decrease until 2.5 Myr, followed by an expansion and then remains almost constant.

Comparing Fig. 4 and Fig. 5, after 7 Myr, more than 600 stars have escaped from the cluster. The most massive object increases its mass to more than $5000 M_{\odot}$. The black hole formation efficiency increases by 5%. Until 2.5 Myr, the system is still very stable so there are very few stellar collisions and escapers. The stellar system goes through contraction after ~ 3 Myr, therefore the largest increase of the most massive object in mass through stellar collisions occurs after this time.

Model M lost only a small fraction of its initial mass due to the stars that escape from the system, around 8%. This stellar system shows few collisions before 2.5 Myr, forming a massive object of $1670 M_{\odot}$. At this time there is a small contraction, so after 2.5 Myr the number of collisions increases and several of them occur with the most massive object which increases in mass, reaching a mass of $6700 M_{\odot}$ yet this star system shows a black hole formation efficiency of only 8% after 10 Myr.

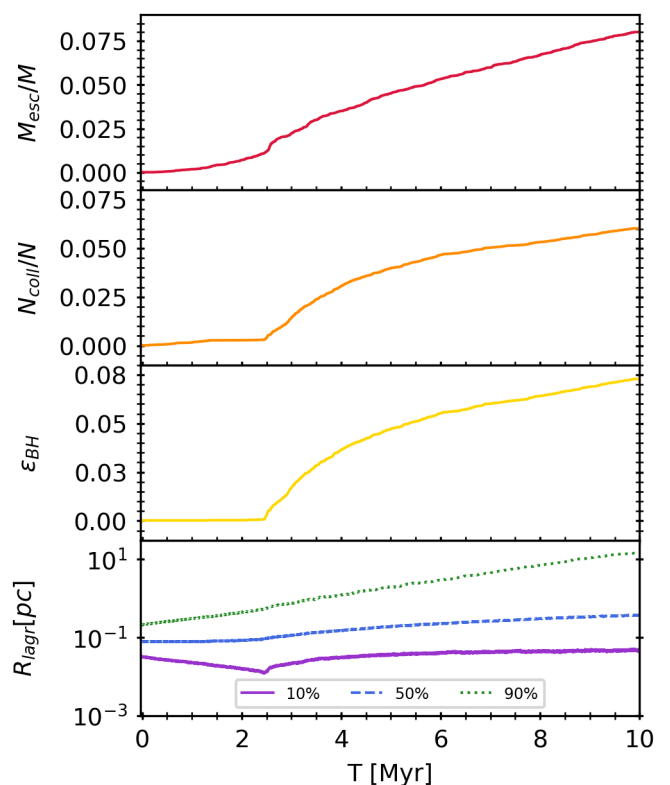


Fig. 5. Evolution of model M for a time period of 10 Myr. Panels are the same as in Fig. 2.

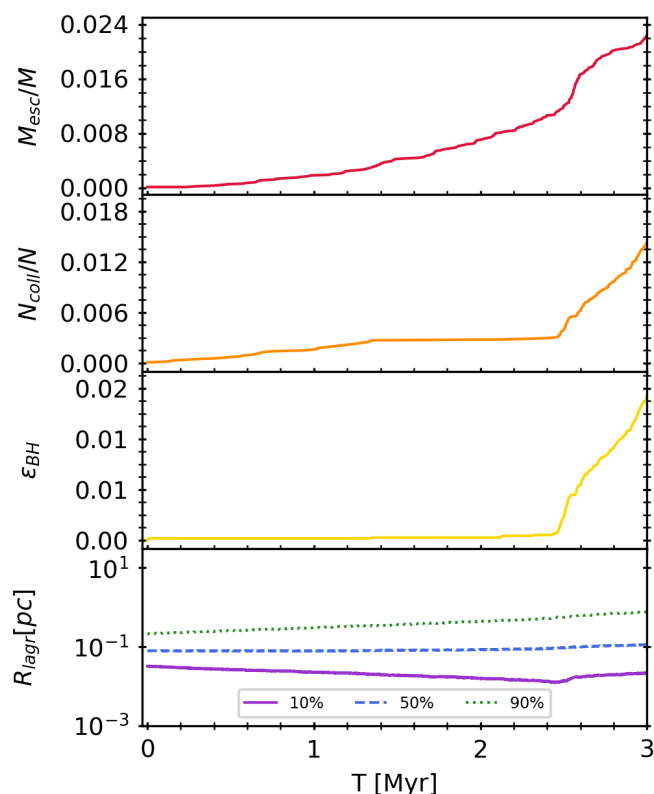


Fig. 4. Evolution of model M for 3 Myr. Panels are the same as in Fig. 2.

Stellar gravitational interactions can cause stars to be ejected from the cluster, taking kinetic energy with them and causing

the cluster energy to redistribute, leading the cluster to undergo contraction. This collapse of the stellar system is related to the formation of the most massive object since the stars are more likely to collide with each other, therefore there is an increase in the number of collisions. At the same time many of these collisions occur with a single object.

Model M is more massive than model B, but also has a larger virial radius, forming a more massive object than model B; nonetheless, its evolution is less chaotic because the collision time scale of model B is shorter than t_H , while model M has a collision time scale larger than t_H . This can be observed in Fig. 1, since the models are in a different part of the mass-radius parameters space; model B is in a region where the collisions dominate the stellar dynamics, while model M is in a region where stellar collisions are avoided. Also, the chaotic gravitational interaction of model B shows a larger fraction of initial mass loss due to stellar escapers than model M. This means that model B has a higher black hole formation efficiency than model M, while nonetheless model M forms a more massive object than model B.

4.2. Black hole formation efficiency

In this subsection, we analyze the black hole formation efficiency (ϵ_{BH}) for the 18 different initial conditions (Table 1), in order to test the scenario for MBH formation proposed by Escala (2021). Our results are based on the average of three simulations for each of the 18 initial conditions configurations, with a different random seed to obtain reliable statistics and error estimates.

On the right side of Fig. 6 (A), we display the black hole formation efficiency as a function of the initial mass of the NSCs. At first glance, there seem to be three trends; according to the colors, they are ordered as orange, magenta, and blue from left

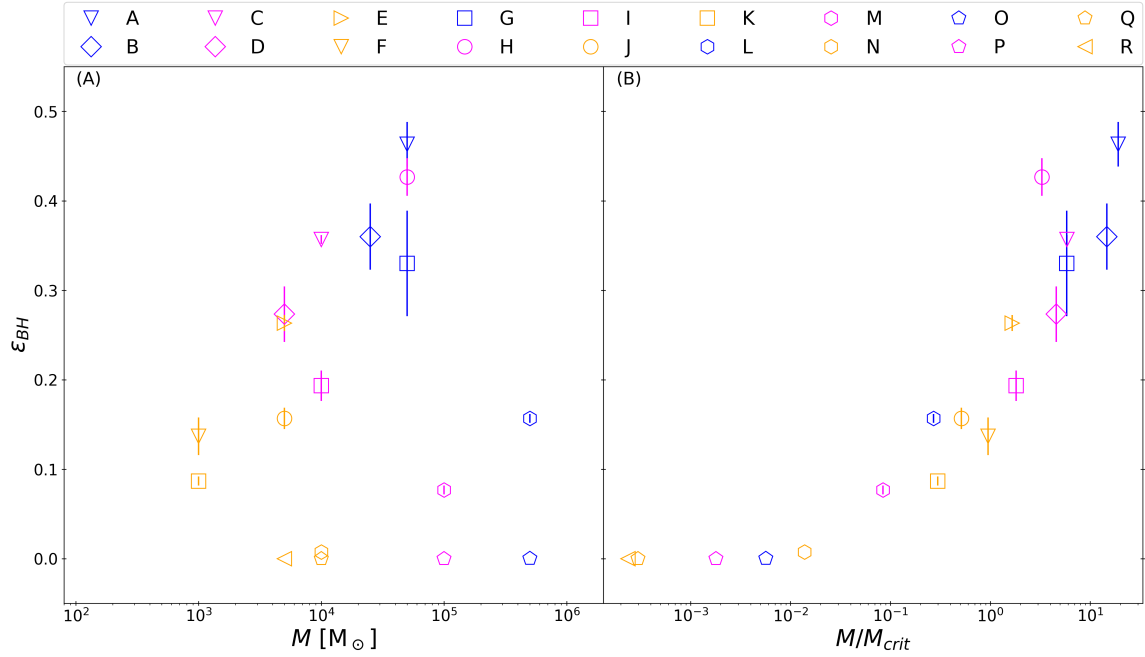


Fig. 6. The right side of Fig. 6 (A) is the black hole efficiency computed by $\epsilon_{BH} = (1 + M_{NSC}/M_{BH})^{-1}$ (eq. 8) for 10 Myr against the initial mass of the nuclear star cluster M . The left side of Fig. 6 (B) is the black hole efficiency computed by equation 8 against the initial mass of the nuclear star cluster M normalized by the critical mass M_{crit} (equation 3) for $t_H = 10$ Myr.

to right. However in order to test the global instability proposed by Escala (2021), it is useful to normalize by the critical mass (M_{crit}); we use this mass to normalize the mass of the clusters, since we need to quantify how near or far away they are from the collision line in Fig. 1.

On the left side of Fig. 6 (B), we display the black hole formation efficiency against the initial mass of the nuclear cluster normalized by the critical mass (M_{crit}) at 10 Myr. The normalization by critical mass is helpful to show a clear trend in the efficiency of black hole formation, where the models with the highest efficiency are also the models where the collision time scale is shorter than t_H and the models with lower black hole formation efficiency are those which have a collision time scale larger than t_H . Model A shows the highest efficiency of around 46%. Model B has $\epsilon_{BH} \approx 36\%$. Models C and D show a black hole formation efficiency of around 35% and 27%, respectively. Models E and F have $\epsilon_{BH} \approx 27\%$ and $\epsilon_{BH} \approx 15\%$, respectively. Model G shows efficiency of around 33%. Model H has $\epsilon_{BH} \approx 44\%$. Model I has $\epsilon_{BH} \approx 19\%$. Models J and K show a black hole formation efficiency of around 17% and 9%, respectively. Models L and M show $\epsilon_{BH} \approx 16\%$, and $\epsilon_{BH} \approx 8\%$, respectively. The black hole formation efficiency is less than 1% for models O and N. $\epsilon_{BH} = 0\%$ for models P, Q, and R.

According to Fig. 1 we described different regions of the mass-radius parameter space (Fig. 1). Models in the region where the collision time is longer than the simulation time (t_H) show the lowest black hole formation efficiencies e.g. models O, P, Q, and R with $\approx 0\%$, including model N with $\sim 1\%$, so in this region collisions are almost entirely avoided. Models K and M show a slightly higher, but still low black hole formation efficiency, reaching values less than 10%. They still are in the parameter space where $t_{coll} > t_H$ but show a bit more collisions since the ratio between the timescales is reduced. They are followed by models F, I, J and L which show a black hole formation efficiency of less than 20%. They are near the lines described

by the collision equation 1. When the collision time is shorter than the simulation time (t_H) the clusters show the highest black hole formation efficiency where collisions dominate the stellar dynamics of the system, e.g models D and E with a black hole formation efficiency larger than 20%; also models B, C, and G show a black hole formation efficiency above 30% and models A and H have a black hole formation efficiency of around 50%. Note that the error bar for the black hole formation efficiency for models N and O is quite small (practically zero) and models P, Q, and R do not show an error bar due these systems do not have collisions.

We summarize our results in Table 2. We provide in the first column the model ID, in the second column the cumulative mass of the escapers (M_{esc}), in the third column the final black hole mass (M_{BH}), in the fourth column the final mass of the nuclear star cluster (M_{NSC}), in the fifth column the final mass of the central massive object (M_{CMO}) and the black hole formation efficiency (ϵ_{BH}) is in the last column.

5. Conclusions

In this work, we investigated the behavior of nuclear stellar clusters and their ability to form massive black holes under runaway collisions, testing the global collapse scenario presented in Escala (2021); we analyzed the Lagrangian radii, the mass loss due to stars escaping from the system, the number of stellar collisions and the black hole formation efficiency.

We performed an analysis of 18 different models covering different regions of the mass-radius parameter space, described in Fig 1. If $t_{coll} < t_H$, the stellar system becomes unstable under collisions, causing a chaotic collapse, ejecting several stars and forming a massive object. On the other hand, if $t_{coll} > t_H$, the system practically avoids almost all of the collisions and experiences very few escapes. When the system is closer to the curve defined by equation 2, fewer collisions will occur, while if the

Table 2. M_{esc} is the cumulative mass of the escapers, the final black hole mass is M_{BH} , M_{NSC} is the final mass of the nuclear star cluster, M_{CMO} is the sum of M_{BH} and M_{NSC} , and the black hole formation efficiency is $\epsilon_{BH} = (1 + M_{NSC}/M_{BH})^{-1}$. All quantities are measured for a time period of 10 Myr. For the cases marked with *, an error estimate was not possible, as all conducted simulations produced the same result. While the uncertainty in these cases should be low, a precise quantification was not feasible.

Models ID	M_{esc} [M_{\odot}]	M_{BH} [M_{\odot}]	M_{NSC} [M_{\odot}]	M_{CMO} [M_{\odot}]	ϵ_{BH}
A	28533 ± 1477	9917 ± 143	11550 ± 1353	21467 ± 1477	46.33 ± 2.5%
B	14300 ± 687	3850 ± 324	6850 ± 795	10700 ± 687	36.00 ± 3.7%
C	5370 ± 42	1660 ± 14	2970 ± 57	4630 ± 42	35.67 ± 0.5%
D	2767 ± 111	610 ± 43	1623 ± 153	2233 ± 111	27.33 ± 3.1%
E	2061 ± 56	778 ± 20	2161 ± 71	2939 ± 56	26.33 ± 0.9%
F	372 ± 5	85 ± 12	542 ± 16	628 ± 5	13.67 ± 2.1%
G	26183 ± 1569	7800 ± 788	16017 ± 2357	23817 ± 1569	33.00 ± 5.9%
H	23137 ± 1966	11397 ± 143	15380 ± 1722	26863 ± 1966	42.67 ± 2.1%
I	4253 ± 183	1110 ± 83	4637 ± 252	5747 ± 183	19.33 ± 1.7%
J	1459 ± 22	545 ± 42	2996 ± 64	3541 ± 22	15.67 ± 1.2%
K	327 ± 8	59 ± 2	614 ± 10	673 ± 8	8.67 ± 0.5%
L	75517 ± 1812	67450 ± 2585	357433 ± 2121	424883 ± 1812	15.67 ± 0.5%
M	7850 ± 283	6987 ± 246	85163 ± 130	92150 ± 283	7.67 ± 0.5%
N	234 ± 44	71 ± 5	9695 ± 49	9766 ± 44	0.73 ± 0.0%
O	450 ± 178	100 ± 0*	499450 ± 178	499550 ± 178	0.02 ± 0.0%
P	27 ± 17	0 ± 0*	99973 ± 17	99973 ± 17	0.00 ± 0.0%*
Q	0 ± 0*	0 ± 0*	10000 ± 0*	10000 ± 0*	0.00 ± 0.0%*
R	0 ± 0*	0 ± 0*	5000 ± 0*	5000 ± 0*	0.00 ± 0.0%*

model is closer to the curve from equation 1, more collisions will happen. The goal of this work was to provide a proof of concept of the critical transition derived by Escala (2021); for computational reasons we could not model real nuclear star clusters with masses of the order $10^7 M_{\odot}$, but we considered smaller and more compact systems following shorter evolutionary times, leading overall to a reduction of the critical mass scale to $10^3 - 10^5 M_{\odot}$ which made the numerical modeling feasible.

We define the efficiency ϵ_{BH} as the ratio of black hole mass to final stellar mass. The models with more chaotic evolution show that at the beginning the black hole formation efficiency is dominated by the stellar collisions, while at late times, the increase of the black hole formation efficiency is quickly dominated by the mass loss due to stellar escapes.

Systems in the region where collisions are avoided have a longer relaxation time; these systems expand rapidly before there is time for collisions to occur, showing a very low black hole formation efficiency that in some cases can be equal to zero. On the other hand, the systems in the region where the collisions are relevant do not have enough time to expand before the collisions dominate the stellar dynamics, forming a very massive object in the center and reaching high black hole formation efficiencies. The extreme models A and H have the same initial mass of $5 \times 10^4 M_{\odot}$, with a viral radius of 0.005 pc and 0.01 pc, respectively; these systems form a massive object of $M_{BH} \approx 10^4 M_{\odot}$ and lose around of 50 – 60% of the initial mass due to the escapers. The black hole formation efficiency of these systems are $\epsilon_{BH} \approx 50\%$, which is the highest of all our models. On the other hand, models where collisions are avoided show a low black hole formation efficiency; particularly models P, Q and R have a long relaxation time so they take longer to core collapse and until the end of our simulations they show no collisions (i.e. the black hole formation efficiency is 0%). There are systems that do not cross the line described by equation 1 but are close to it (e.g models B, C, D, E, and G). These show a black hole formation efficiency higher than 20 – 30% while other systems (e.g F, I, J, K, L, and M) further away from the collision line show lower black hole formation efficiencies of around 10 – 20%. We find,

that the black hole formation efficiency is high in the parameter space where the collisions are relevant for the global instability, and the violent behavior of the NSC before the cluster expansion allows the formation of a MBH, besides that in our simulations $t_{relax} < t_{coll}$, leading to a even simpler scenario and more similar to the one originally proposed in Escala (2020). Here we explored setups where $t_H = 10$ Myr, with the ideal conditions to be only proof of concept of global collapse triggered by collisions.

So the occurrence of a transition in the black hole formation efficiency was clearly demonstrated within our toy models. As mentioned above, in real NSCs the critical mass scale will be larger of the order $10^7 M_{\odot}$, and they also have larger masses of up to a few $10^8 M_{\odot}$. Assuming that a black hole formation efficiency of 50% is possible, such systems could potentially form supermassive black holes with up to $\sim 10^8 M_{\odot}$. The Universe has an age of 13.6 Gyr, which means that even more extended systems with longer collision and relaxation time scales can go through this global collapse.

Some studies suggest that massive seeds ($\sim 10^5 M_{\odot}$) are needed to explain the observed supermassive black holes at high redshift (Pezzulli et al. 2016; Valiante et al. 2016; Sassano et al. 2021; Trinca et al. 2022). Our chaotic models reach black hole masses of the order of $10^3 - 10^4 M_{\odot}$ even in the idealized simulations, results consistent with the simulations of Portegies Zwart & McMillan (2002); Devecchi & Volonteri (2009); Sakurai et al. (2017); Reinoso et al. (2018). In realistic more massive systems in principle the formation of even more massive central objects is thus expected. In general we expect that for dense models where the parameter space is dominated by collisions higher black hole masses are reached when the long available times are taken into account ($> 10^5 M_{\odot}$) (Lee 1987; Quinlan & Shapiro 1990; Davies et al. 2011; Stone et al. 2017). If NSCs are born with a radius such that their initial mass is $10 M_{crit}$, they can lead to the formation of massive objects of $\sim 10^5 M_{\odot}$ assuming a 50% efficiency.

Eventually observations of NSCs with the James Webb Space Telescope (JWST)² will be possible at high redshift ($3 \leq z \leq 8$) (Renzini 2017), and similar for the Extremely Large Tele-

² JWST: <https://webb.nasa.gov>

scope (ELT)³ which will be equipped with MICADO, the Multi-AO Imaging Camera for Deep Observations at near-infrared wavelengths. The high spatial resolution of MICADO will allow the spheres of influence to be resolved with greater precision, considerably increasing the available surveys of supermassive black holes masses covering a black hole mass range of $10^5 - 10^7 M_{\odot}$ (Davies et al. 2018). The high spatial resolution of MICADO will allow to resolve the sphere of influence at a 5 times larger distance than the current instruments, also 2 times larger than the JWST. MICADO will observe many additional NSCs and determine many supermassive black hole masses that will allow the efficiency of black hole formation to be determined with high precision. The large observational data set could be compared with the results of our models. Our models suggests that NSCs could form a more massive object than $10^5 M_{\odot}$ through runaway collisions. It is difficult to make direct observations of the formation process of MBH, especially in this stellar compact configuration, gravitational waves are also expected to occur at the galactic center (Rees 1984), thus the detection of gravitational waves using LISA⁴ will deliver important information on this process (Amaro-Seoane et al. 2022). These observations will also help to probe the new formation scenario proposed here, by providing an accurate estimation of black hole masses for a large range of different clusters.

5.1. Potential caveats for future improvement

As mentioned, NSCs live in the center of galaxies and it has been suggested that the formation of NSCs is due to the accretion of globular clusters, which fall to the center by dynamic friction (Antonini et al. 2012). This mechanism is called a cluster-inspiral and is generally invoked as an explanation for the rotation observed in NSCs (Seth et al. 2008). Therefore, including rotation in NSC simulations will be important when developing more realistic simulations, since the presence of rotation in the spherical models leads to a deformation in the outer zone of the cluster, appearing in a non-spherical distribution (Varri & Bertin 2012; Lupton & Gunn 1987). Rotation in stellar systems slightly reduces collisions due to the ordered motion, however, rotation also causes a flattening of the cluster, increasing the density and number of collisions (Vergara et al. 2021).

Another important simplification in this work is to simulate clusters only with equal mass stars. Stellar populations are complex since they are born with an initial distribution of the masses of their stars that is called the initial mass function (IMF) (Salpeter 1955). The IMF is similar within the Milky Way and nearby star-forming regions (Kroupa 2001; Chabrier 2003). Including the IMF also implies considering mass segregation, as massive objects tend to fall toward the center while light objects move outward (Baumgardt et al. 2008), which explains the depletion of low-mass stars (Aarseth & Woolf 1972). The evolution of clusters depends strongly on their primordial binaries since a small fraction of binary systems can play a crucial role in the dynamics of the clusters (Goodman & Hut 1989; Portegies Zwart et al. 2001).

Our simulations do not take into account stellar evolution, so our NCSs are dominated by gravity. However, it is important to consider that due to the mass loss produced by stellar winds and supernova explosions, these winds lead to a strong expansion at the beginning of the cluster evolutionary process (~ 10 Myr) (Applegate 1986; Chernoff & Shapiro 1987; Chernoff & Wein-

berg 1990; Fukushige & Heggie 1995). Due to mass segregation, the most massive stars or stellar black holes sink into the cluster center, where the stars often form hard binaries with high eccentricities, implying that this dense stellar configuration is a source of gravitational waves, so it is necessary to use post-Newtonian N-body dynamics to successfully solve this scenario, as done for example in the works of Blanchet et al. (2006); Brem et al. (2013); Rizzuto et al. (2021, 2022); Arca-Sedda et al. (2021).

Numerical simulations of a large number of particles require a lot of time and computational resources. However, this scenario was investigated with the DRAGON simulations of globular clusters with 10^6 stars (Wang et al. 2016) using `NBODY6++GPU` (Wang et al. 2015). With this background, it is possible to explore this new proposed runaway collision scenario in NSCs as a mechanism to form MBHs (Escala 2021) for a greater number of stars ($N = 10^5 - 10^6$), that is, more massive clusters ($\sim 10^6 - 10^8 M_{\odot}$) and thus more supermassive black holes ($\sim 10^6 - 10^7 M_{\odot}$).

Including gas in NSCs is another interesting option, especially at higher redshifts, where gas in galaxies can account for up to 80% of the baryonic mass for some extreme cases (Molina et al. 2019). The dissipative nature of gas should enhance stellar collision, for example through dynamical friction (Ostriker 1999; Escala et al. 2004) but the presence of gas in a cluster could also delay the formation of a MBH due to stellar collisions, since stars reach higher velocities, so it is more difficult for close encounters to occur. These systems also have a longer relaxation time; however if the simulation is long enough these systems could form a MBH, since the gas limits the expansion of the cluster, allowing more stars to remain in the cluster thus forming a more massive MBH than a gasless system (Reinoso et al. 2020). Also the high density in systems with gas must allow the formation of MBH with masses of the order $\leq 10^5 M_{\odot}$ (Davies et al. 2011). Quite similarly, the interaction between the gas and the protostars can also lead to the formation of massive objects (Boekholt et al. 2018; Schleicher et al. 2022).

Acknowledgements. MCV acknowledge funding through ANID (Doctorado acuerdo bilateral DAAD/62210038) and DAAD (funding program number 57600326). MCV, DRGS and AE acknowledge financial support from Millennium Nucleus NCN19_058 (TITANs) and also support from the Center for Astrophysics and Associated Technologies CATA (FB210003). AE also acknowledge financial support from FONDECYT Regular grant #1181663. DRGS also acknowledge financial support from FONDECYT Regular grant #1201280. BR acknowledges funding through ANID (CONICYT-PFCHA/Doctorado acuerdo bilateral DAAD/62180013) and DAAD (funding program number 57451854). These resources made the presented work possible, by supporting its development.

References

- Aarseth, S. J. 2000, *The Chaotic Universe*, 286. doi:10.1142/9789812793621_0019
- Aarseth, S. J. & Woolf, N. J. 1972, *Astrophys. Lett.*, 12, 159
- Ahmad, A. & Cohen, L. 1973, *Journal of Computational Physics*, 12, 389. doi:10.1016/0021-9991(73)90160-5
- Akiyama, K., Alberdi, A., Alef, W., et al. 2022, *ApJ*, 930, L14. doi:10.3847/2041-8213/ac6429
- Alistair Seguel, P. J., Schleicher, D. R. G., Boekholt, T. C. N., et al. 2020, *MNRAS*, 493, 2352. doi:10.1093/mnras/staa456
- Amaro-Seoane, P., Andrews, J., Arca Sedda, M., et al. 2022, arXiv:2203.06016
- Antonini, F., Capuzzo-Dolcetta, R., Mastrobuono-Battisti, A., et al. 2012, *ApJ*, 750, 111. doi:10.1088/0004-637X/750/2/111
- Antonini, F., Barausse, E., & Silk, J. 2015, *ApJ*, 812, 72. doi:10.1088/0004-637X/812/1/72
- Applegate, J. H. 1986, *ApJ*, 301, 132. doi:10.1086/163881
- Arca-Sedda, M., Rizzuto, F. P., Naab, T., et al. 2021, *ApJ*, 920, 128. doi:10.3847/1538-4357/ac1419

³ ELT: <https://elt.eso.org>

⁴ LISA: <https://lisa.nasa.gov>

- Banerjee, S. & Kroupa, P. 2017, *A&A*, 597, A28. doi:10.1051/0004-6361/201526928
- Barnes, J. E. 2002, *MNRAS*, 333, 481. doi:10.1046/j.1365-8711.2002.05335.x
- Barth, A. J., Strigari, L. E., Bentz, M. C., et al. 2009, *ApJ*, 690, 1031. doi:10.1088/0004-637X/690/1/1031
- Baumgardt, H., De Marchi, G., & Kroupa, P. 2008, *ApJ*, 685, 247. doi:10.1086/590488
- Baumgardt, H., Amaro-Seoane, P., & Schödel, R. 2018, *A&A*, 609, A28. doi:10.1051/0004-6361/201730462
- Bañados, E., Venemans, B. P., Decarli, R., et al. 2016, *ApJS*, 227, 11. doi:10.3847/0067-0049/227/1/11
- Bañados, E., Venemans, B. P., Mazzucchelli, C., et al. 2018, *Nature*, 553, 473. doi:10.1038/nature25180
- Begelman, M. C. 2010, *MNRAS*, 402, 673. doi:10.1111/j.1365-2966.2009.15916.x
- Bender, R., Kormendy, J., Bower, G., et al. 2005, *ApJ*, 631, 280. doi:10.1086/432434
- Binney, J. & Tremaine, S. 2008, *Galactic Dynamics: Second Edition*, Princeton University Press, Princeton, NJ USA, 2008.
- Blanchet, L., Buonanno, A., & Faye, G. 2006, *Phys. Rev. D*, 74, 104034. doi:10.1103/PhysRevD.74.104034
- Boekholt, T. C. N., Schleicher, D. R. G., Fellhauer, M., et al. 2018, *MNRAS*, 476, 366. doi:10.1093/mnras/sty208
- Bond, J. R., Arnett, W. D., & Carr, B. J. 1984, *ApJ*, 280, 825. doi:10.1086/162057
- Bovino, S., Grassi, T., Schleicher, D. R. G., et al. 2016, *ApJ*, 832, 154. doi:10.3847/0004-637X/832/2/154
- Brem, P., Amaro-Seoane, P., & Spurzem, R. 2013, *MNRAS*, 434, 2999. doi:10.1093/mnras/stt1220
- Bromm, V. & Loeb, A. 2003, *ApJ*, 596, 34. doi:10.1086/377529
- Böker, T., Laine, S., van der Marel, R. P., et al. 2002, *AJ*, 123, 1389. doi:10.1086/339025
- Böker, T. 2008, *Journal of Physics Conference Series*, 131, 012043. doi:10.1088/1742-6596/131/1/012043
- Chabrier, G. 2003, *PASP*, 115, 763. doi:10.1086/376392
- Chernoff, D. F. & Shapiro, S. L. 1987, *ApJ*, 322, 113. doi:10.1086/165708
- Chernoff, D. F. & Weinberg, M. D. 1990, *ApJ*, 351, 121. doi:10.1086/168451
- Cohn, H. 1979, *ApJ*, 234, 1036. doi:10.1086/157587
- Côté, P., Piatek, S., Ferrarese, L., et al. 2006, *ApJS*, 165, 57. doi:10.1086/504042
- Davies, M. B., Benz, W., & Hills, J. G. 1993, *ApJ*, 411, 285. doi:10.1086/172828
- Davies, M. B., Miller, M. C., & Bellovary, J. M. 2011, *ApJ*, 740, L42. doi:10.1088/2041-8205/740/2/L42
- Davies, R., Alves, J., Clénet, Y., et al. 2018, *Proc. SPIE*, 10702, 107021S. doi:10.1117/12.2311483
- Demircan, O. & Kahraman, G. 1991, *Ap&SS*, 181, 313. doi:10.1007/BF00639097
- Devecchi, B. & Volonteri, M. 2009, *ApJ*, 694, 302. doi:10.1088/0004-637X/694/1/302
- Elmegreen, B. G., Bournaud, F., & Elmegreen, D. M. 2008, *ApJ*, 684, 829. doi:10.1086/590361
- Escala, A., Larson, R. B., Coppi, P. S., et al. 2004, *ApJ*, 607, 765. doi:10.1086/386278
- Escala, A. 2006, *ApJ*, 648, L13. doi:10.1086/507988
- Escala, A. 2007, *ApJ*, 671, 1264. doi:10.1086/523092
- Escala, A. 2020, arXiv:2006.01826v1
- Escala, A. 2021, *ApJ*, 908, 57. doi:10.3847/1538-4357/abd93c
- Event Horizon Telescope Collaboration, Akiyama, K., Alberdi, A., et al. 2019, *ApJ*, 875, L1. doi:10.3847/2041-8213/ab0ec7
- Fan, X., Strauss, M. A., Schneider, D. P., et al. 2003, *AJ*, 125, 1649. doi:10.1086/368246
- Ferrarese, L. & Merritt, D. 2000, *ApJ*, 539, L9. doi:10.1086/312838
- Ferrarese, L., Côté, P., Dalla Bontà, E., et al. 2006, *ApJ*, 644, L21. doi:10.1086/505388
- Filippenko, A. V. & Ho, L. C. 2003, *ApJ*, 588, L13. doi:10.1086/375361
- Freitag, M. & Benz, W. 2005, *MNRAS*, 358, 1133. doi:10.1111/j.1365-2966.2005.08770.x
- Fukushige, T. & Heggge, D. C. 1995, *MNRAS*, 276, 206. doi:10.1093/mnras/276.1.206
- Genzel, R., Eisenhauer, F., & Gillessen, S. 2010, *Reviews of Modern Physics*, 82, 3121. doi:10.1103/RevModPhys.82.3121
- Georgiev, I. Y., Böker, T., Leigh, N., et al. 2016, *MNRAS*, 457, 2122. doi:10.1093/mnras/stw093
- Ghez, A. M., Salim, S., Weinberg, N. N., et al. 2008, *ApJ*, 689, 1044. doi:10.1086/592738
- Gieles, M., Moeckel, N., & Clarke, C. J. 2012, *MNRAS*, 426, L11. doi:10.1111/j.1745-3933.2012.01312.x
- Gillessen, S., Plewa, P. M., Eisenhauer, F., et al. 2017, *ApJ*, 837, 30. doi:10.3847/1538-4357/aa5c41
- Goodman, J. & Hut, P. 1989, *Nature*, 339, 40. doi:10.1038/339040a0
- Graham, A. W. & Spitler, L. R. 2009, *MNRAS*, 397, 2148. doi:10.1111/j.1365-2966.2009.15118.x
- Gültekin, K., Richstone, D. O., Gebhardt, K., et al. 2009, *ApJ*, 698, 198. doi:10.1088/0004-637X/698/1/198
- Häring, N. & Rix, H.-W. 2004, *ApJ*, 604, L89. doi:10.1086/383567
- Katz, H., Sijacki, D., & Haehnelt, M. G. 2015, *MNRAS*, 451, 2352. doi:10.1093/mnras/stv01048
- King, A. 2016, *MNRAS*, 456, L109. doi:10.1093/mnras/456/l109
- Kormendy, J. & Ho, L. C. 2013, *ARA&A*, 51, 511. doi:10.1146/annurev-astro-082708-101811
- Kroupa, P. 2001, *MNRAS*, 322, 231. doi:10.1046/j.1365-8711.2001.04022.x
- Kustaanheimo, P. & Stiefel, E. 1965, *J. Reine Angew. Math.*, 218, 204
- Landau, L. D. & Lifshitz, E. M. 1980, *Course of theoretical physics*, Oxford: 3rd rev. and enlarg. ed.
- Latif, M. A., Omukai, K., Habouzit, M., et al. 2016, *ApJ*, 823, 40. doi:10.3847/0004-637X/823/1/40
- Latif, M. A. & Schleicher, D. R. G. 2015, *A&A*, 578, A118. doi:10.1051/0004-6361/201525855
- Latif, M. A., Schleicher, D. R. G., Schmidt, W., et al. 2013, *MNRAS*, 436, 2989. doi:10.1093/mnras/stt1786
- Lee, H. M. 1987, *ApJ*, 319, 801. doi:10.1086/165498
- Leigh, N., Böker, T., & Knigge, C. 2012, *MNRAS*, 424, 2130. doi:10.1111/j.1365-2966.2012.21365.x
- Li, Y., Haiman, Z., & Mac Low, M.-M. 2007, *ApJ*, 663, 61. doi:10.1086/518398
- Lupton, R. H. & Gunn, J. E. 1987, *AJ*, 93, 1106. doi:10.1086/114394
- Lützgendorf, N., Kissler-Patig, M., Noyola, E., et al. 2011, *A&A*, 533, A36. doi:10.1051/0004-6361/201116618
- Lynden-Bell, D. & Wood, R. 1968, *MNRAS*, 138, 495. doi:10.1093/mnras/138.4.495
- Magorrian, J., Tremaine, S., Richstone, D., et al. 1998, *AJ*, 115, 2285. doi:10.1086/300353
- Makino, J. 1991, *ApJ*, 369, 200. doi:10.1086/169751
- Marconi, A. & Hunt, L. K. 2003, *ApJ*, 589, L21. doi:10.1086/375804
- Mayer, L., Kazantzidis, S., Escala, A., et al. 2010, *Nature*, 466, 1082. doi:10.1038/nature09294
- Mikkola, S. & Aarseth, S. J. 1990, *Celestial Mechanics and Dynamical Astronomy*, 47, 375
- Mikkola, S. & Aarseth, S. J. 1993, *Celestial Mechanics and Dynamical Astronomy*, 57, 439. doi:10.1007/BF00695714
- J Molina, Edo Ibar, I Smail, A M Swinbank, E Villard, A Escala, D Sobral, T M Hughes, The kiloparsec-scale gas kinematics in two star-forming galaxies at $z \sim 1.47$ seen with ALMA and VLT-SINFONI, *Monthly Notices of the Royal Astronomical Society*, Volume 487, Issue 4, August 2019, Pages 4856–4869
- Mortlock, D. J., Warren, S. J., Venemans, B. P., et al. 2011, *Nature*, 474, 616. doi:10.1038/nature10159
- Natarajan, P. & Treister, E. 2009, *MNRAS*, 393, 838. doi:10.1111/j.1365-2966.2008.13864.x
- Neumayer, N., Seth, A., & Böker, T. 2020, *A&A Rev.*, 28, 4. doi:10.1007/s00159-020-00125-0
- Nguyen, D. D., Seth, A. C., den Brok, M., et al. 2017, *ApJ*, 836, 237. doi:10.3847/1538-4357/aa5cb4
- Nguyen, D. D., Bureau, M., Thater, S., et al. 2022, *MNRAS*, 509, 2920. doi:10.1093/mnras/stab3016
- Jiang, N., Wang, T., Zhou, H., et al. 2018, *ApJ*, 869, 49. doi:10.3847/1538-4357/aaeb90
- Nitadori, K. & Aarseth, S. J. 2012, *MNRAS*, 424, 545. doi:10.1111/j.1365-2966.2012.21227.x
- Omukai, K., Schneider, R., & Haiman, Z. 2008, *ApJ*, 686, 801. doi:10.1086/591636
- Omukai, K. & Nishi, R. 1998, *ApJ*, 508, 141. doi:10.1086/306395
- Ostriker, E. C. 1999, *ApJ*, 513, 252. doi:10.1086/306858
- Pacucci, F., Natarajan, P., & Ferrara, A. 2017, *ApJ*, 835, L36. doi:10.3847/2041-8213/835/2/L36
- Panamarev, T., Just, A., Spurzem, R., et al. 2019, *MNRAS*, 484, 3279. doi:10.1093/mnras/stz208
- Pezzulli, E., Valiante, R., & Schneider, R. 2016, *Active Galactic Nuclei 12: A Multi-Messenger Perspective (AGN12)*, 6. doi:10.5281/zenodo.163523
- Plummer, H. C. 1911, *MNRAS*, 71, 460. doi:10.1093/mnras/71.5.460
- Portegies Zwart, S. F., McMillan, S. L. W., Hut, P., et al. 2001, *The Influence of Binaries on Stellar Population Studies*, 264, 371. doi:10.1007/978-94-015-9723-4_27
- Portegies Zwart, S. F., Makino, J., McMillan, S. L. W., et al. 1999, *A&A*, 348, 117
- Portegies Zwart, S. F. & McMillan, S. L. W. 2002, *ApJ*, 576, 899. doi:10.1086/341798
- Prieto, J. & Escala, A. 2016, *MNRAS*, 460, 4018. doi:10.1093/mnras/stw1285
- Prieto, J., Escala, A., Privon, G. C., et al. 2021, *MNRAS*, 508, 3672. doi:10.1093/mnras/stab2740
- Quinlan, G. D. & Shapiro, S. L. 1990, *ApJ*, 356, 483. doi:10.1086/168856

- Rees, M. J. 1984, *ARA&A*, 22, 471. doi:10.1146/annurev.aa.22.090184.002351
- Reinoso, B., Schleicher, D. R. G., Fellhauer, M., et al. 2018, *A&A*, 614, A14. doi:10.1051/0004-6361/201732224
- Reinoso, B., Schleicher, D. R. G., Fellhauer, M., et al. 2020, *A&A*, 639, A92. doi:10.1051/0004-6361/202037843
- Renzini, A. 2017, *MNRAS*, 469, L63. doi:10.1093/mnras/slx057
- Ricarte, A. & Natarajan, P. 2018, *MNRAS*, 481, 3278. doi:10.1093/mnras/sty2448
- Rizzuto, F. P., Naab, T., Spurzem, R., et al. 2021, *MNRAS*, 501, 5257. doi:10.1093/mnras/staa3634
- Rizzuto, F. P., Naab, T., Spurzem, R., et al. 2022, *MNRAS*, 512, 884. doi:10.1093/mnras/stac231
- Rossa, J., van der Marel, R. P., Böker, T., et al. 2006, *AJ*, 132, 1074. doi:10.1086/505968
- Sakurai, Y., Hosokawa, T., Yoshida, N., et al. 2015, *MNRAS*, 452, 755. doi:10.1093/mnras/stv1346
- Sakurai, Y., Yoshida, N., & Fujii, M. S. 2019, *MNRAS*, 484, 4665. doi:10.1093/mnras/stz315
- Sakurai, Y., Yoshida, N., Fujii, M. S., et al. 2017, *MNRAS*, 472, 1677. doi:10.1093/mnras/stx2044
- Salpeter, E. E. 1955, *ApJ*, 121, 161. doi:10.1086/145971
- Sassano, F., Schneider, R., Valiante, R., et al. 2021, *MNRAS*, 506, 613. doi:10.1093/mnras/stab1737
- Schleicher, D. R. G., Reinoso, B., Latif, M., et al. 2022, *MNRAS*, 512, 6192. doi:10.1093/mnras/stac926
- Schleicher, D. R. G., Palla, F., Ferrara, A., et al. 2013, *A&A*, 558, A59. doi:10.1051/0004-6361/201321949
- Schödel, R., Feldmeier, A., Neumayer, N., et al. 2014, 31, 244007. doi:10.1088/0264-9381/31/24/244007
- Seth, A. C., Blum, R. D., Bastian, N., et al. 2008, *ApJ*, 687, 997. doi:10.1086/591935
- Seth, A. C., Cappellari, M., Neumayer, N., et al. 2010, *ApJ*, 714, 713. doi:10.1088/0004-637X/714/1/713
- Shields, J. C., Walcher, C. J., Böker, T., et al. 2008, *ApJ*, 682, 104. doi:10.1086/589680
- Shlosman, I., Begelman, M. C., & Frank, J. 1990, *Nature*, 345, 679. doi:10.1038/345679a0
- Shu, F. H. 1991, *The physics of astrophysics. Volume 1: Radiation*. University Science Books.
- Spitzer, L. 1969, *ApJ*, 158, L139. doi:10.1086/180451
- Spitzer, L. 1987, Princeton, N.J.: Princeton University Press, c1987.
- Spurzem, R. 1999, *Journal of Computational and Applied Mathematics*, 109, 407
- Stone, N. C., Küpper, A. H. W., & Ostriker, J. P. 2017, *MNRAS*, 467, 4180. doi:10.1093/mnras/stx097
- Suazo, M., Prieto, J., Escala, A. & Schleicher, DRG, *ApJ*, 885, 127. doi:10.3847/1538-4357/ab45eb
- Tan, J. C. & McKee, C. F. 2004, *ApJ*, 603, 383. doi:10.1086/381490
- Tremaine, S., Gebhardt, K., Bender, R., et al. 2002, *ApJ*, 574, 740. doi:10.1086/341002
- Trinca, A., Schneider, R., Valiante, R., et al. 2022, *MNRAS*, 511, 616. doi:10.1093/mnras/stac062
- Valiante, R., Schneider, R., Volonteri, M., et al. 2016, *Active Galactic Nuclei 12: A Multi-Messenger Perspective (AGN12)*, 4. doi:10.5281/zenodo.163515
- Varri, A. L. & Bertin, G. 2012, *A&A*, 540, A94. doi:10.1051/0004-6361/201118300
- Vergara, M. Z. C., Schleicher, D. R. G., Boekholt, T. C. N., et al. 2021, *A&A*, 649, A160. doi:10.1051/0004-6361/202140298
- Volonteri, M. 2010, *A&A Rev.*, 18, 279. doi:10.1007/s00159-010-0029-x
- Volonteri, M., Lodato, G., & Natarajan, P. 2008, *MNRAS*, 383, 1079. doi:10.1111/j.1365-2966.2007.12589.x
- Volonteri, M., Haardt, F., & Madau, P. 2003, *ApJ*, 582, 559. doi:10.1086/344675
- Walcher, C. J., van der Marel, R. P., McLaughlin, D., et al. 2005, *ApJ*, 618, 237. doi:10.1086/425977
- Wang, L., Spurzem, R., Aarseth, S., et al. 2015, *MNRAS*, 450, 4070. doi:10.1093/mnras/stv817
- Wang, L., Spurzem, R., Aarseth, S., et al. 2016, *MNRAS*, 458, 1450. doi:10.1093/mnras/stw274
- Wehner, E. H. & Harris, W. E. 2006, *ApJ*, 644, L17. doi:10.1086/505387
- Woods, T. E., Agarwal, B., Bromm, V., et al. 2019, *PASA*, 36, e027. doi:10.1017/pasa.2019.14
- Wu, X.-B., Wang, F., Fan, X., et al. 2015, *Nature*, 518, 512. doi:10.1038/nature14241